Cumhuriyet Sci. J., 46(3) (2025) 957-963
DOI: https://doi.org/10.17776/csj.1703812

Cumhuriyet Science Journal

| csj.cumhuriyet.edu.tr | Founded: 2002 ISSN: 2587-2680 e-ISSN: 2587-246X Publisher: Sivas Cumhuriyet University

Simulation Study on The Sorting of Chiral Active Brownian Colloids By Optical Barriers

Harun Yücel [1, a,*]

[1]Bayburt Üniversitesi, Sağlık Hizmetleri Meslek Yüksekokulu, Tıbbi Hizmetler ve Teknikler Bölümü, Optisyenlik Programı, 69000, Bayburt, Türkiye

*Corresponding author

Research Article

History
Received: 21/05/2025
Accepted: 04/11/2025

ABSTRACT

This study considers the dynamics of chiral active Brownian particles (CABPs) through numerical simulations conducted under the influence of an optical field. Unlike passive Brownian particles, CABPs possess a propulsion mechanism and a chiral torque that induce curved trajectories, complex motion, and out-of-equilibrium behavior. These properties make CABPs interesting for both theoretical research and potential applications in the control of active matter. In simulations, CABPs are modeled as spherical particles with a refractive index suspended in a fluid medium (water). When illuminated by an optical field, these particles experience optical forces due to the momentum transfer from the light field, which affects their motion. This interaction provides a powerful method for guiding, confining, or sorting them based on their motile characteristics. As a result, the study demonstrates that optical fields can serve as both static and dynamic barriers, significantly influencing the trajectories of particles. The findings present that optical landscapes can separate and orient CABPs based on their propulsion speed and chirality. The study emphasizes the potential of optical manipulation as a tunable technique for chiral active particles in complex environments.

Keywords: Active colloids, Chirality, Optical fields, Particle motion

[a] harunyucel@bayburt.edu.tr https://orcid.org/0000-0001-9406-0220

Introduction

Active colloids, which convert internal energy into directed motion [1], have emerged as a key topic in physics, chemistry, and biology due to their complex dynamics [2]. Unlike passive Brownian particles, whose random motion results from thermal collisions with fluid molecules [3,4], active particles exhibit self-propulsion and experience forces and torques that drive them out of thermal equilibrium [5–7]. This behavior is reminiscent of biological systems, such as bacteria and cells, as well as synthetic microswimmers like Janus particles [8–10].

Active particles are generally classified into three types [11]. The first, known as active Brownian particles (ABPs), exhibit self-propelled motion at a speed v along straight trajectories, interrupted by random reorientations, often due to thermal fluctuations [5,12]. The second type, chiral active Brownian particles (CABPs), move with both a self-propulsion speed, v, and an intrinsic angular velocity, Ω [13]. Their trajectories form circles in two dimensions or helices in three dimensions, with a well-defined chirality. This motion, first discussed by Lord Kelvin in 1893, is observed in systems ranging from bacteria and biomolecules to artificial microswimmers [14,15]. The third type, known as spinners, is characterized by pure rotational motion at a constant Ω without translational self-propulsion [16].

Understanding CABP dynamics is crucial for the development of particle manipulation techniques [17], particularly for sorting microswimmers based on properties such as self-propulsion and chirality [18,19]. In the literature, several sorting strategies have been proposed involving mechanisms such as (i) clustering and phase separation [20–22], (ii) directed motion [23–26], and (iii) interactions with structured obstacles. In particular, chiral swimmers of opposite handedness can be separated via geometrical traps, including flower-shaped patterns [27], counter-rotating obstacles [28], asymmetric L-shaped arrays [29], and spiral structures [30].

Recently, the interaction of active particles with optical fields has attracted considerable attention [31,32]. Light-matter interactions, through momentum transfer, can alter the trajectories of active particles, offering a tunable tool for controlling their behavior [33,34]. Optical fields can be designed to trap, guide, and sort active particles based on differences in physical properties, such as size, refractive index, propulsion speed, and rotational diffusion [35–37].

This study investigates the dynamics of CABPs in structured optical fields via numerical simulations. By analyzing the trajectories resulting from interactions with optical fields, the study demonstrates that light patterns can affect particles as both static and dynamic obstacles, allowing control over CABP motion. In particular, the simulations show that low-intensity regions of light fields behave as a practical obstacle. In contrast, high-intensity regions of patterns can guide particles into desired areas and trap them selectively based on their dynamic properties. Furthermore, it is demonstrated that optical patterns with geometrical features, such as flower-shaped fields, can facilitate the separation of CABPs based on their self-propulsion speed and chirality under both steady and time-varying conditions.

While previous studies have relied on physical obstacles to manipulate active particles, this work demonstrates that structured optical fields can achieve similar or even more effective results. Optical fields are easier to generate, can form dynamic, moving barriers and allow for selective control based on particle properties, such as chirality and angular velocity.

These findings not only enhance the understanding of CABP dynamics in complex environments but also show the potential of optical manipulation as a powerful platform for controlling active matter. The results could pave the way for designing advanced sorting and transport mechanisms in applications ranging from drug delivery in microfluidic systems to the study of collective behavior in biological and synthetic microswimmer populations.

Material and Methods

This study uses computer simulations to understand the behavior of active particles under optical force fields. The particles are considered to be spherical in shape, transparent, with a refractive index n_p, and suspended in a liquid with a refractive index n_m. The medium surrounding the particles is assumed to be illuminated with a parallelly oriented optical pattern, $\mathrm{I}(\mathrm{M},\mathrm{N})$, pixelated into M rows and N columns. Due to the optical field, an optical force field occurs, exerting a force on the particles. The optical force can be calculated using the following equation [38] (see Figures 1(a) and 1 (b)

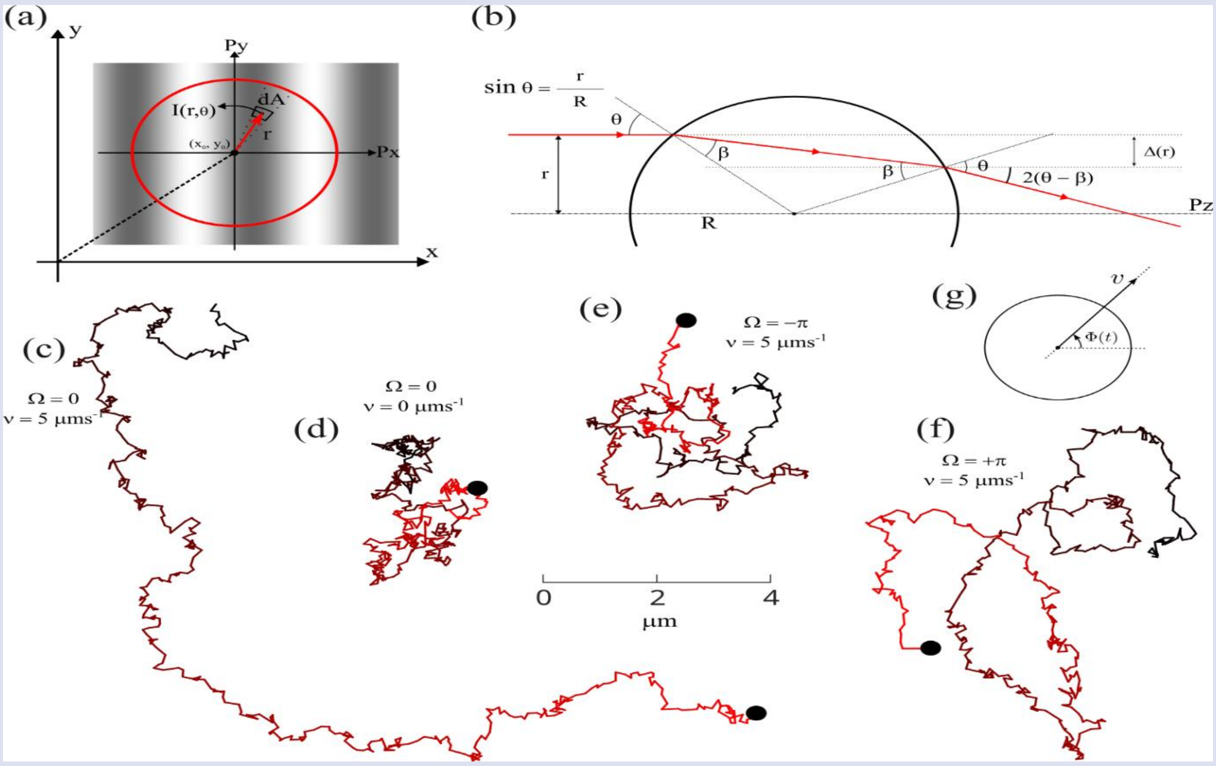

Figure 1. (a) illustrates the coordinates of the simulation system along with an optical light field. x and y are axes of the sample chamber referance frame (the lab refrence frame). The red circle represents the cross-sectional area of the particle in 2D. The point (x_0, y_0) is the position of the particle in the lab reference frame. dA denotes a unit area on the cross-sectional area of the particle in the particle referance frame. r and θ are the polar coordinates on the particle cross-sectional area. (b) geometrically defines Δr for the refraction of a single ray through the particle. (d) shows the trajectories of a $1\ \mu\mathrm{m}$ diameter particle, which corresponds to Brownian motion ($\Omega = 0$ and $v = 0$). (e) and (f) show the trajectories for chiral active particles with opposite angular velocity ($\Omega = \pm\pi$, $v = 5\ \mu\mathrm{ms}^{-1}$) while (c) shows the trajectories of an active Brownian particle ($\Omega = 0, v = 5\ \mu\mathrm{ms}^{-1}$). In the Figure (c--f), the colors of the trajectory lines change from black to red, corresponding to the progression from the starting time to the end. (g) represents an active Brownian particle that is characterized by an orientation $\Phi(t)$ and a self-propulsion speed v.

$$\boldsymbol{F} = \boldsymbol{\kappa}\int_0^R\int_0^{2\pi} \mathbf{I}(\boldsymbol{r},\boldsymbol{\theta})\boldsymbol{\Delta r}\, \boldsymbol{rdrd\theta} \qquad (1)$$

Here, the parameter κ is a conversion factor that relates the grayscale intensity of the pattern to the light power. $dA = rdrd\theta$ corresponds to the cross-sectional area of the particle. Δr represents the vertical distance between the encounter point of the incident ray and the outgoing point of the refracted ray on the particle (see Figure 1 (b)) and is expressed in the following form

$$\boldsymbol{\Delta r} = \frac{\boldsymbol{r}}{\boldsymbol{R}}\sqrt{\mathbf{1} - \left(\frac{\boldsymbol{r}}{\boldsymbol{nR}}\right)^{\mathbf{2}}} - \frac{\boldsymbol{r}}{\boldsymbol{nR}}\sqrt{\mathbf{1} - \left(\frac{\boldsymbol{r}}{\boldsymbol{R}}\right)^{\mathbf{2}}} \qquad (2)$$

Here, r represents the distance from the particle center, and R is the radius of the particle. n corresponds to the ratio of n_p/n_m.

In addition to the parameters of Brownian particles in simulations, active particles are characterized by three additional parameters: angular velocity (Ω), self-propulsion speed (v), and the orientation (Φ) of the particle with respect to the sample chamber reference frame (see Figure 1 (g)). The trajectories of the particles are generated by the numerical solution of the Langevin equation with the added optical force, as follows [6,7,39]

$$\begin{aligned} \boldsymbol{\Phi_i} &= \boldsymbol{\Phi_{i-1}} + \boldsymbol{\Omega\Delta t} + \sqrt{\boldsymbol{2D_R\Delta t}}\boldsymbol{\omega_\Phi} \\ \boldsymbol{x_i} &= \boldsymbol{x_{i-1}} + \boldsymbol{v}\cos(\boldsymbol{\Phi_{i-1}})\,\boldsymbol{\Delta t} + \boldsymbol{Fx_{i-1}}\,\boldsymbol{\Delta t/\gamma} \\ &\qquad + \sqrt{\boldsymbol{2D_T\Delta t}}\boldsymbol{\omega_x} \\ \boldsymbol{y_i} &= \boldsymbol{y_{i-1}} + \boldsymbol{v}\sin(\boldsymbol{\Phi_{i-1}})\,\boldsymbol{\Delta t} + \boldsymbol{Fy_{i-1}}\,\boldsymbol{\Delta t/\gamma} \\ &\qquad + \sqrt{\boldsymbol{2D_T\Delta t}}\boldsymbol{\omega_y} \end{aligned} \tag{3}$$

Here, i represents the step index in the discretized time sequence of the simulation. $\gamma = 6\pi\eta R$, $D_T = K_b T/\gamma$ translational diffusion coefficient and $D_R = 0.75 D_T/R^2$ rotational diffusion coefficient. $\eta = 1\ \text{fN}/\mu\text{m}^2$ is the viscosity of the liquid, $T = 300$ K is the temperature and $K_b = 0.0138\ \text{fN}\mu\text{mK}^{-1}$ is Boltzmann constant. ω_Φ, ω_x, and ω_y are white noise (Wiener process) with zero (0) mean and unit (1) variance for the x, y, and Φ components separately. In all simulations in the study, the interactions between particles and hydrodynamic interactions were ignored.

A simulation platform was developed in MATLAB based on the above formulation. This platform is a revised version of simLightForce, adapted to account for the behavior of an active Brownian particle (see [40]). A series of simulations was conducted for a 1 μm diameter silica particle ($n_p = 1.59$) suspended in water ($n_m = 1.33$) without any optical pattern at 100 frames per second (fps) for 5 seconds to evaluate its performance. In these simulations, various angular velocities (Ω) and self-propulsion speeds (v) were considered. The resulting trajectories are presented in Figure 1 (c) active Brownian motion, (d) Brownian motion (passive), chiral active Brownian motion (e) in the clockwise direction, and (f) in the anticlockwise direction. The results are consistent with those reported in [7].

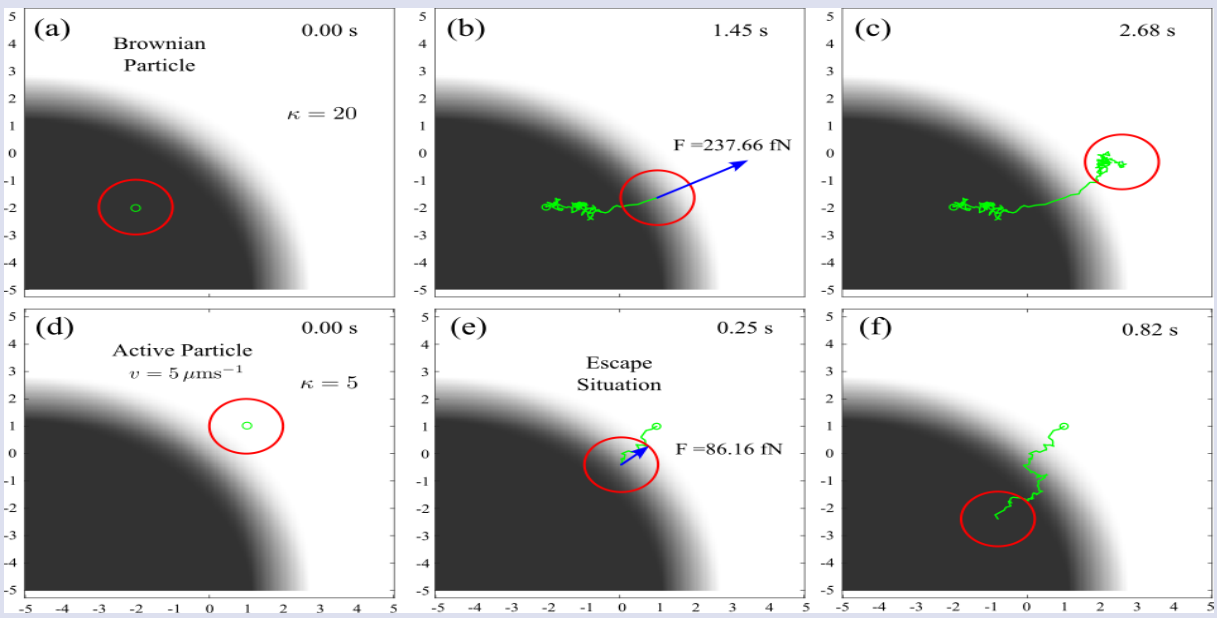

Figure 2. The figure presents sequences taken during simulations conducted for a 2 μm diameter particle under an optical field containing white and black regions. (a--c) show the trajectories of a 2 μm diameter Brownian particle and the optical force (F) exerted on it. The κ parameter for the optical field is 20, corresponding to a high optical power, resulting in a strong optical gradient force on the particle. This force restricts the particle in the white region. The particle cannot re-enter the black region. (d--e) show the trajectories of an active Brownian particle with a self-propulsion speed of $v = 5\ \mu\text{ms}^{-1}$. The κ parameter for the optical field is 5, corresponding to weak optical power and a weak optical gradient force. This force is not sufficient to keep the particle in the white region due to the high energy of the active Brownian particle. As a result, the particle can escape into the black region

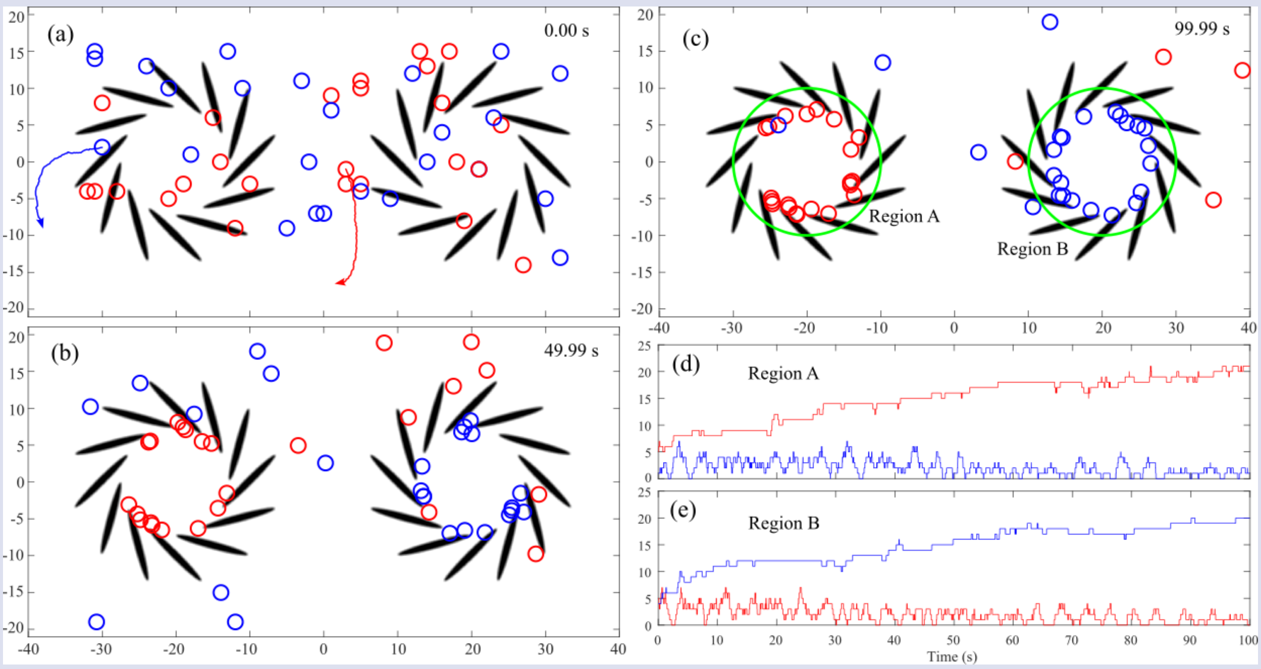

Figure 3. The figure presents simulation results for active chiral particles with opposite chiralities in a flower-shaped optical field (see (Mijalkov & Volpe, 2013; Volpe et al., 2014)). In the simulation, the particles have a diameter of 2 μm, a self-propulsion speed of $v = 20\ \mu\mathrm{ms}^{-1}$, and an angular velocity of $\Omega = +\pi / 2$ (anticlockwise) for the blue particles and $\Omega = -\pi / 2$ (clockwise) for the red particles. (a--c) present sequences from the simulation. (d) and (e) show the number of particles as a function of time in regions A and B, respectively, which are marked by green circles in (c).

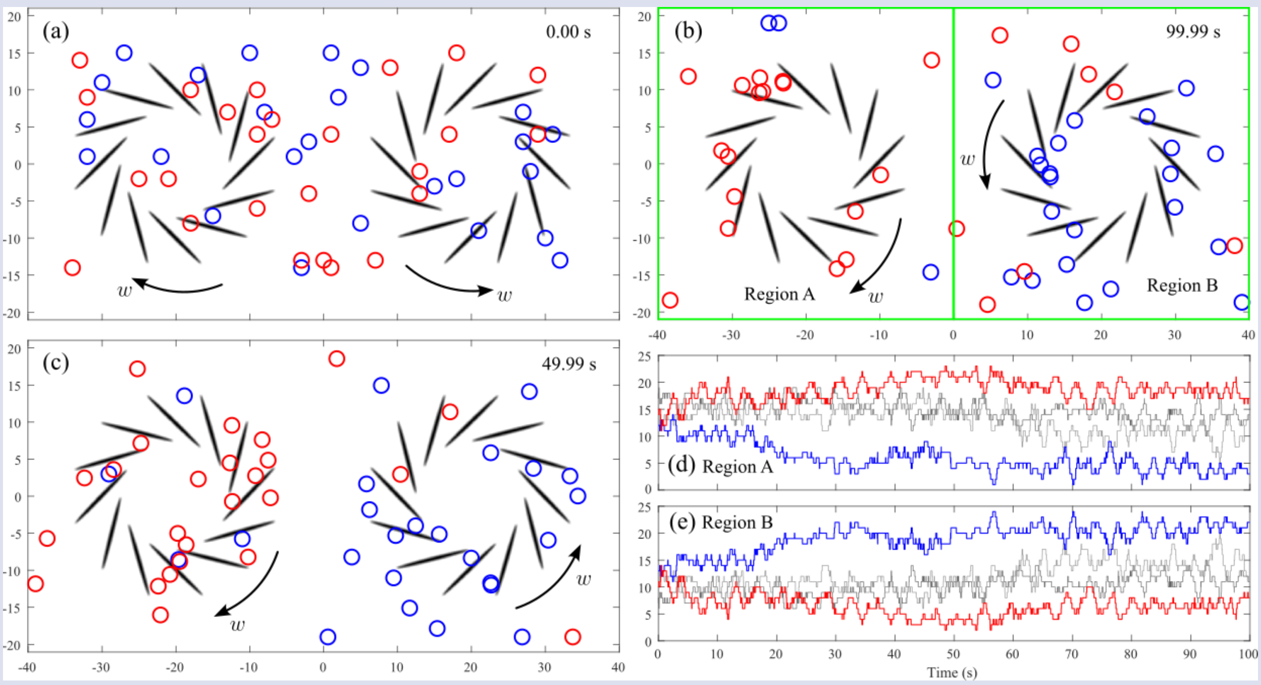

Figure 4. The figure presents simulation results for active chiral particles with opposite chiralities in a flower-shaped optical field that rotates with angular velocity w (see (Chen & Ai, 2015)). The left flower rotates clockwise with $w = -\pi / 2$ while the right flower rotates anticlockwise with $w = +\pi / 2$. In the simulation, the particles have a diameter of 2 μm, a self-propulsion speed of $v = 20\ \mu\mathrm{ms}^{-1}$, and an angular velocity of $\Omega = +\pi / 2$ (anticlockwise) for the blue particles and $\Omega = -\pi / 2$ (clockwise) for the red particles. (a--c) present sequences from the simulation. (d) and (e) show the number of particles as a function of time in regions A and B, respectively, which are marked by green rectangles in (c). In the graphics, the gray lines represent the number of particles for the performed simulation with the same parameters without any optical field.

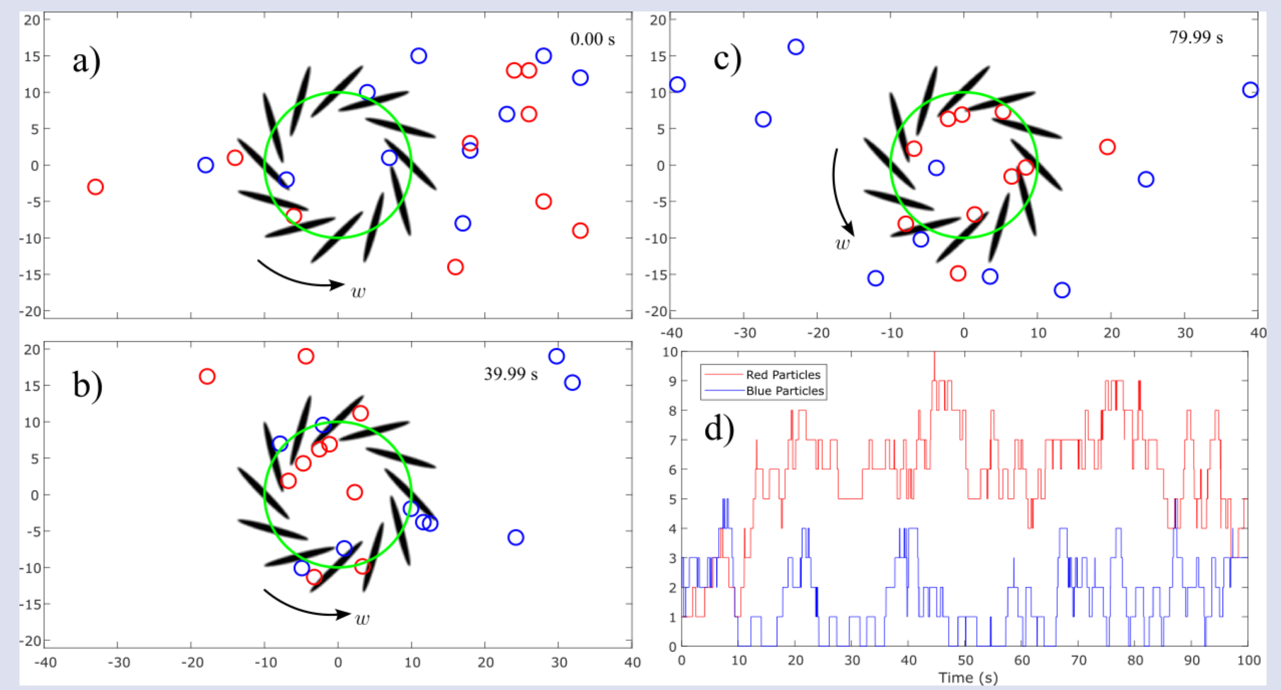

Figure 5. The figure presents simulation (for angular-velocity-selective behavior) results for active chiral particles with the same chirality but different magnitudes in a single flower-shaped optical field rotating with angular velocity w. The flower rotates anticlockwise with $w = +\pi / 4$. In the simulation, the particles have a diameter of 2 μm, a self-propulsion speed of $v = 20\ \mu ms^{-1}$, and an angular velocity of $\Omega = +\pi / 4$ (anticlockwise, equal to the flower) for the blue particles and $\Omega = +\pi / 2$ (anticlockwise) for the red particles. Panels (a–c) present sequences from the simulation, and panel (d) shows the number of particles as a function of time in the flower's area, which is marked by green circles in panels (a–c).

Results and Discussions

To investigate the behavior of an active particle in an optical light field, a series of simulations was conducted using an optical pattern composed of low- and high-intensity regions. The light power of the optical field was characterized by the parameter $\kappa = 20$. The considered particle was a 2 μm diameter silica particle ($n_p = 1.59$) suspended in water ($n_m = 1.33$), with its motion recorded at 100 frames per second (fps) for 5 seconds. As a baseline, the first simulation was performed for a purely Brownian particle, i.e., without self-propulsion or angular velocity. Figure 2 (a--c) shows the simulation sequences over time. In the simulation, the particle starts its motion in the low-intensity (black) region. When it reaches the border between low- and high-intensity regions, it undergoes an optical force due to the intensity gradient at the boundary. The direction of this force is always toward the high-intensity region as a result of the light gradient at the interface. The maximum force exerted on the particle is 237.66 fN. This amount is generally sufficient to keep the particle in a high-intensity region, depending on the light power, and prevents it from re-entering a low-intensity region. Therefore, it can be concluded that a low-intensity region in an optical pattern behaves as an obstacle. When the simulation is repeated with only self-propulsion set to $v = 5\ \mu ms^{-1}$ and the light power parameter set to $\kappa = 5$, the particle appears to re-enter a low-intensity region because the maximum optical force (86.166 fN) is too weak to prevent it, as can be seen in Figure 2 (d--f). In the second simulation, the particle's internal energy is high due to self-propulsion, and the light power is too low to generate a strong intensity gradient force. Therefore, under appropriate conditions, it can be said that a low-intensity region behaves as an obstacle for active Brownian particles.

In the following simulation, a mixture of chiral active particles with opposite chirality was considered. The optical pattern was designed as chiral flowers with opposite chiralities, as implemented in [7, 27], providing an accumulation of chiral particles with different chiralities in distinct flower-shaped areas.

The dimensions of the flower pattern were determined based on the particle diameter and the expected trajectory radius of the particles. For example, by ignoring thermal fluctuations, a chiral active particle with a self-propulsion speed v and an angular velocity Ω follows a circular orbit with a radius $R_{orbit} = v/\Omega$. To ensure that the particles remain inside the flower pattern, the pattern radius should be larger than the expected orbit radius. Other pattern parameters, such as the number of petals, were selected based on the particle diameter. Moreover, a detailed definition and similar simulations for different particle sizes can be found in the literature, as discussed in [27].

The simulation was conducted for 50 particles, consisting of a mixture of 25 particles with an angular velocity of $\Omega = +\pi / 2$ (anticlockwise) and 25 particles with $\Omega = -\pi / 2$ (clockwise), all having a diameter of 2 μm, a self-propulsion speed of $v = 20\ \mu ms^{-1}$. The κ parameter was set to 20 for generating the optical light pattern, and the simulation was performed at 100 frames per second (fps) for 100 seconds.

Figure 3 (a--c) shows sequences from the simulation. Initially, the particles are randomly distributed in the sample chamber, but over time, they accumulate in accordance with the chirality of the flower pattern. When observing the number of particles within the flower patterns (see Figure 3 (d) and (e)), the number of particles with $\Omega = +\pi\ /\ 2$ chirality (the blue particles) increases in the right flower. In contrast, the number of particles with $\Omega = -\pi\ /\ 2$ chirality (the red particles) increases in the left flower over time.

An advantage of using optical fields to influence particle motion is the ability to avoid hydrodynamic forces. Optical obstacles enable the creation and design of more complex and time-varying structures. Thus, a simulation with a flower-shaped optical pattern, where the flower rotates with an angular velocity (w), was conducted for the particles used in the previous simulation. Figure 4 (a--e) presents the results of this simulation.

At this point, the chiralities of the flower-shaped patterns are important. When the rotation speed is high, the influence of the pattern decreases. However, when the chirality of the flower pattern matches the chirality of the particles, a different accumulation effect is observed in the sample chamber (see [28]). As seen in Figure 4 (a--c), the density of the particles increases around the rotating flower, in contrast to the accumulation inside the flowers. Over time, the number of red particles ($\Omega = -\pi\ /\ 2$) increases on the left side of the chamber, while the number of blue particles ($\Omega = +\pi\ /\ 2$) increases on the right side of the chamber. Figure 4 (d) and (e) show the number of particles in the left and right sides of the chamber, respectively. In addition, the gray lines in the graphs represent the number of particles on the left and right sides when the simulation was repeated without any optical pattern. This simulation shows that chiral particles spend more time around the rotating flower or any obstacle that has the same angular velocity as the particles.

During the study, many simulations were performed with various rotational angular velocities of the pattern. It was observed that when the rotation of the pattern is slower than the particles' angular velocity, the particles accumulate inside the flower-shaped region. However, when the rotation of the pattern is faster than that of the particles, the influence of the pattern becomes inefficient, and the particles move as if there were no optical field. Moreover, the influence of rotation has been discussed in [28] for physical obstacles used for crossing.

The last simulation presented above shows that when the rotation speed of the flower-shaped pattern equals the particles' angular velocity, the particles do not accumulate within the flower. In this manner, an additional simulation can be designed to separate a mixture of particles with the same chirality but different angular velocities. For this purpose, $2\ \mu m$ diameter particles with a self-propulsion speed of $v = 20\ \mu m s^{-1}$ were considered, having angular velocities of $\Omega = +\pi\ /\ 4$ (anticlockwise) for 10 particles (blue particles in Figure 5) and $\Omega = +\pi\ /\ 2$ (anticlockwise) for 10 particles (red particles in Figure 5). The flower-shaped optical field was positioned at the center of the sample chamber, with petals exhibiting the opposite chirality to that of the particles. The rotation speed (w) of the flower pattern was adjusted to $\Omega = +\pi\ /\ 4$ (matching that of the blue particles). Thus, the pattern rotates relatively slower for the particles with $\Omega = +\pi\ /\ 2$, allowing the red particles to accumulate within the flower. Figure 5 (a–c) shows sequential frames from the simulation, while Figure 5 (d) presents the number of particles as a function of time within the flower region, where the particle concentration is high.

Conclusion

In this study, the motions of active chiral particles under an optical field were investigated by numerical simulations. The results demonstrated that optical fields can affect particles as both static and dynamic obstacles, which considerably influence the trajectories and spatial distribution of CABPs. It has been demonstrated that light-induced potential landscapes enable selective control over particle motion, allowing for tasks such as trapping, guiding, and sorting based on physical properties like self-propulsion speed and chirality. Especially, flower-shaped optical patterns were found to effectively separate CABPs not only with opposite chiralities but also with the same chirality and different angular velocities under rotating field configurations.

In particular, flower-shaped optical patterns effectively separated CABPs with opposite chirality in static and time-dependent field configurations. These findings provide new insights into the complex interaction between active matter and external fields, underscoring the potential of optical manipulation for the controlled self-assembly and separation of microswimmers in various applications.

This work contributes to the understanding of active matter systems. It offers a promising strategy for future experiments to harness light fields to precisely control self-propelled particles in biological, chemical, and soft-matter environments.

Author Contribution

The entire process of the article was carried out by HY.

Declaration Of Ethical Code

The author declares that this study does not require ethical committee approval or any legal permission.

Conflicts Of Interest

The author declares no conflicts of interest.

Data Availability

The raw data supporting the conclusions of this article will be made available by the author on request.

References

[1] Ramaswamy S., The Mechanics and Statistics of Active Matter, *Annual Review of Condensed Matter Physics*, 1 (2010) 323–45.

[2] Marchetti M. C., Joanny J. F., Ramaswamy S., Liverpool T. B., Prost J., Rao M. and Simha R. A., Hydrodynamics of soft active matter, *Rev. Mod. Phys*., 85 (2013) 1143–89.

[3] Erdmann U., Ebeling W., Schimansky-Geier L. and Schweitzer F., Brownian particles far from equilibrium, *Eur. Phys. J. B*, 15 (2000) 105–13.

[4] Hagen B. ten, Teeffelen S. van and Löwen H., Brownian motion of a self-propelled particle, *J. Phys.: Condens. Matter,* 23 (2011) 194119.

[5] Basu U., Majumdar S. N., Rosso A. and Schehr G., Active Brownian motion in two dimensions, *Phys. Rev. E*, 98 (2018) 062121.

[6] Callegari A. and Volpe G., Numerical Simulations of Active Brownian Particles, *Flowing Matter ed: F Toschi and M Sega (Cham: Springer International Publishing)*, (2019) pp 211–38.

[7] Volpe G., Gigan S. and Volpe G., Simulation of the active Brownian motion of a microswimmer, *American Journal of Physics*, 82 (2014) 659–64.

[8] Bechinger C., Di Leonardo R., Löwen H., Reichhardt C., Volpe G. and Volpe G., Active particles in complex and crowded environments, *Rev. Mod. Phys.,* 88 (2016) 045006.

[9] Elgeti J., Winkler R. G. and Gompper G., Physics of microswimmers—single particle motion and collective behavior: a review, *Rep. Prog. Phys*., 78 (2015) 056601.

[10] Gompper G., Bechinger C., Herminghaus S., Isele-Holder R., Kaupp U. B., Löwen H., Stark H. and Winkler R. G., Microswimmers – From Single Particle Motion to Collective Behavior, *Eur. Phys. J. Spec. Top*., 225 (2016) 2061–4.

[11] Liebchen B. and Levis D., Chiral active matter, *EPL*, 139 (2022) 67001.

[12] Babič D., Schmitt C. and Bechinger C., Colloids as model systems for problems in statistical physics, *Chaos: An Interdisciplinary Journal of Nonlinear Science*, 15 (2005) 026114.

[13] Sevilla F. J., Diffusion of active chiral particles, *Phys. Rev. E*, 94 (2016) 062120.

[14] Berg H. C., E. coli in Motion, New York NY: Springer, (2004).

[15] Tailleur J. and Cates M. E., Statistical Mechanics of Interacting Run-and-Tumble Bacteria, *Phys. Rev. Lett*., 100 (2008) 218103.

[16] Libet P. A., Yakovlev E. V., Kryuchkov N. P., Simkin I. V., Sapelkin A. V. and Yurchenko S. O., Tunable colloidal spinners: Active chirality and hydrodynamic interactions governed by rotating external electric fields, *The Journal of Chemical Physics*, 161 (2024) 044903.

[17] Reichhardt C., Libál A. and Reichhardt C. J. O., Future directions for active matter on ordered substrates, *EPL,* 139 (2022) 27001.

[18] Aristov M., Eichhorn R. and Bechinger C., Separation of chiral colloidal particles in a helical flow field, *Soft Matter*, 9 (2013) 2525–30.

[19] Reichhardt C. J. O. and Reichhardt C., Ratchet Effects in Active Matter Systems, *Annu. Rev. Condens. Matter Phys*. 8 (2017) 51–75.

[20] Ai B-Q., Quan S., and Li. F., Spontaneous demixing of chiral active mixtures in motility-induced phase separation, *New J. Phys*, 25 (2023) 063025.

[21] Li J., Guo R. and Ai B., Spontaneous separation of attractive chiral mixtures, *Phys. Rev. E*, 110 (2024) 024608.

[22] Reichhardt C. and Reichhardt C. J. O., Pattern formation and transport for externally driven active matter on periodic substrates(a), *EPL,* 142 (2023) 37001.

[23] Bag P., Nayak S., Debnath T. and Ghosh P. K., Directed Autonomous Motion and Chiral Separation of Self-Propelled Janus Particles in Convection Roll Arrays, *J. Phys. Chem. Lett*., 13 (2022) 11413–8.

[24] Caprini L., Hernández-García E., López C. and Marini Bettolo Marconi U., A comparative study between two models of active cluster crystals, *Sci Rep*, 9 (2019) 16687.

[25] Chen A., Li G., Luo H., Chen Z., Feng H., Kuang T., An H., Han X., Xiong W. and Xiao G., Effects of detection-beam focal offset on back-focal-plane displacement detection, *AIP Advances,* 14 (2024) 045008.

[26] Nayak S., Das S., Bag P., Debnath T. and Ghosh P. K., Driven transport of active particles through arrays of symmetric obstacles, *The Journal of Chemical Physics*, 159 (2023) 164109.

[27] Mijalkov M. and Volpe G., Sorting of chiral microswimmers, *Soft Matter,* 9 (2013) 6376–81.

[28] Chen Q. and Ai B., Sorting of chiral active particles driven by rotary obstacles, *The Journal of Chemical Physics*, 143 (2015) 104113.

[29] Reichhardt C. and Reichhardt C. J. O., Dynamics and separation of circularly moving particles in asymmetrically patterned arrays, *Phys. Rev. E*, 88 (2013) 042306.

[30] Xu G., Li T-C. and Ai B., Sorting of chiral active particles by a spiral shaped obstacle, *Physica A: Statistical Mechanics and its Applications*, 608 (2022) 128247.

[31] Buttinoni I., Caprini L., Alvarez L., Schwarzendahl F. J. and Löwen H., Active colloids in harmonic optical potentials(a), *EPL,* 140 (2022) 27001.

[32] Caprini L., Löwen H. and Marconi U. M. B., Chiral active matter in external potentials, *Soft Matter,* 19 (2023) 6234–46.

[33] Buttinoni I., Volpe G., Kümmel F., Volpe G. and Bechinger C., Active Brownian motion tunable by light, *J. Phys.: Condens. Matter,* 24 (2012) 284129.

[34] Jahanshahi S., Lozano C., Liebchen B., Löwen H. and Bechinger C., Realization of a motility-trap for active particles, *Commun Phys*, 3 (2020) 1–11.

[35] Li M., Yan S., Zhang Y., Chen X. and Yao B., Optical separation and discrimination of chiral particles by vector beams with orbital angular momentum, *Nanoscale Adv.,* 3 (2021) 6897–902.

[36] Volpe G., Volpe G., Gigan S., Brownian Motion in a Speckle Light Field: Tunable Anomalous Diffusion and Selective Optical Manipulation, *Sci Rep.,* 5 4 (2014) 3936.

[37] Mousavi S.M., Kasianiuk I., Kasyanyuk D., Velu S.K.P., Callegari A., Biancofiore L., Volpe G., Clustering of Janus particles in an optical potential driven by hydrodynamic fluxes. *Soft Matter*, 15 28 (2019) 5748–59.

[38] Sarmiento-Gómez E., Rivera-Morán J. A. and Arauz-Lara J. L., Single particle states of colloidal particles in 2D periodic potentials, *Soft Matter*, 14 (2018) 3684–8.

[39] Volpe G. and Volpe G., Simulation of a Brownian particle in an optical trap, *American Journal of Physics*, 81 (2013) 224–30.

[40] Yücel H., A simulation study on colloid diffusion under time-varying optical potentials, *Journal of Applied Physics*, 134 (2023) 01